HHS Public Access

Author manuscript

Kidney Int. Author manuscript; available in PMC 2018 November 01.

Published in final edited form as:

Kidney Int. 2017 November ; 92(5): 1178–1193. doi:10.1016/j.kint.2017.03.037.

The loss of Krüppel-like factor 15 in Foxd1+ stromal cells exacerbates kidney fibrosis

Xiangchen Gu[1,2,#], **Sandeep K. Mallipattu**[#,3], **Yiqing Guo**[3], **Monica P. Revelo**[4], **Jesse Pace**[3], **Timothy Miller**[3], **Xiang Gao**[1], **Mukesh K. Jain**[5], **Agnieszka B. Bialkowska**[6], **Vincent W. Yang**[6], **John C. He**[7,8], and **Changlin Mei**[1]

[1]Kidney Institute of PLA, Department of Medicine, Changzheng Hospital, Second Military Medical University, Shanghai 200003, People's Republic of China

[2]Department of Nephrology, Yueyang hospital of Integrated Traditional Chinese and Western Medicine, Shanghai University of T.C.M, People's Republic of China

[3]Division of Nephrology, Department of Medicine, Stony Brook University, Stony Brook, NY

[4]Department of Pathology, University of Utah, Salt Lake City, Utah

[5]Case Cardiovascular Research Institute, Department of Medicine, Case Western Reserve University, Cleveland Ohio

[6]Division of Gastroenterology, Department of Medicine, Stony Brook University, Stony Brook, NY

[7]Division of Nephrology, Department of Medicine, Icahn School of Medicine at Mount Sinai, NY, NY

[8]Renal Section, James J. Peters VA Medical Center, New York, NY

Abstract

Large epidemiological studies clearly demonstrate that multiple episodes of acute kidney injury contribute to the development and progression of kidney fibrosis. Although our understanding of kidney fibrosis has improved in the past two decades, we have limited therapeutic strategies to halt its progression. Myofibroblast differentiation and proliferation remain critical to progression of kidney fibrosis. Although canonical Wnt signaling can trigger activation of myofibroblasts in the kidney, mediators of Wnt inhibition in the resident progenitor cells are unclear. Recent studies demonstrate that the loss of a Kruppel-Like Factor 15 (KLF15), a kidney-enriched zinc-finger transcription factor, exacerbates kidney fibrosis in murine models. Here, we tested whether *Klf15*

To whom correspondence should be addressed: Sandeep K. Mallipattu, MD, Department of Medicine/Nephrology, Stony Brook University, 100 Nicolls Road, HSCT17-090B, Stony Brook, NY, USA., Tel: 631-638-2164, Fax: 631-444-6174, sandeep.mallipattu@stonybrookmedicine.edu Or Changlin Mei, MD, Kidney Institute of PLA, Department of Medicine, Changzheng Hospital, Second Military Medical University, Shanghai 200003, People's Republic of China, Tel: 86-21-81885391, Fax: 86-21-81885412, chlmei1954@126.com.

[#]Both authors contributed equally to the work

DISCLOSURES

None

mRNA and protein expression is reduced in late stages of fibrosis in mice that underwent unilateral ureteric obstruction, a model of progressive renal fibrosis Knockdown of *Klf15* in *Foxd1*-expressing cells (*Foxd1-Cre Klf15fl/fl*) increased extracellular matrix deposition and myofibroblast proliferation as compared to wildtype (*Foxd1-Cre Klf15+/+*) mice after three and seven days of ureteral obstruction. This was validated in mice receiving angiotensin II treatment for six weeks. In both these murine models, the increase in renal fibrosis was found in *Foxd1-Cre Klf15fl/fl* mice and accompanied by activation of Wnt/β-catenin signaling. Furthermore, knockdown of *Klf15* in cultured mouse embryonic fibroblasts activated canonical Wnt/β-catenin signaling, increased profibrotic transcripts, and increased proliferation after treatment with a Wnt1 ligand. Conversely, overexpression of *KLF15* inhibited phospho-β-catenin (Ser552) expression in Wnt1-treated cells. Thus, KLF15 has a critical role in attenuating kidney fibrosis by inhibiting the canonical Wnt/β-catenin pathway.

Keywords

Krüppel-like factor; fibroblasts; chronic kidney disease; fibrosis; Wnt/β-catenin signaling

INTRODUCTION

A multitude of factors contribute to the progression of chronic kidney disease (CKD) in humans. Release of profibrotic stimuli from the injured epithelium during kidney injury promotes the differentiation and proliferation of myofibroblasts, which directly contribute to kidney fibrosis [1, 2]. Furthermore, repeated bouts of acute kidney injury result in maladaptive repair that further propagates the activation of myofibroblasts in the renal interstitium [3]. Recent studies have identified progenitor cells in the renal stroma that have the potential to differentiate into myofibroblasts under profibrotic stimuli from the injured epithelium [4]. In addition, many laboratories have reported that paracrine signaling through TGFβ, PDGFRβ, and Wnt/β-catenin in the renal interstitium is critical to the progression of fibrosis in the kidney [2, 5]. Although several studies have reported the potential pathways driving fibrosis, we have limited data on mechanisms that halter or slow the activation of myofibroblasts in the kidney.

Paracrine Wnt/β-catenin signaling remains critical to myofibroblast proliferation and the pathogenesis of kidney fibrosis [6, 7]. Wnt signaling is not only driven by profibrotic stimuli in the renal interstitium, but also directly contributes to CKD progression [7–10]. Furthermore, injured renal tubules release Wnt1, activator of canonical Wnt pathway, which contributes to myofibroblast differentiation [6, 9].

Krüppel-Like Factors (KLFs) are a subclass of zinc-finger family of DNA-binding transcriptional regulators that are involved in a broad range of cellular processes (i.e. cell differentiation, angiogenesis, erythropoiesis) [11–13]. Recent studies demonstrate that KLFs play a vital role in cardiac, liver, and kidney fibrosis [11–13]. Specifically, the global loss of KLF15 exacerbated interstitial fibrosis in 5/6 nephrectomized rats [14, 15]. Although the loss of the KLF15 may contribute to increased extracellular matrix deposition by increasing connective tissue growth factor (CTGF) expression through non-canonical TGFβ

signaling [15], the mechanism by which myofibroblast differentiation occurs remains unclear. In myocardial injury, Wnt/β-catenin mediated cardiac progenitor cell differentiation was regulated by KLF15 [16]. Based on these reported findings, we hypothesize that the loss of KLF15 increases the susceptibility to kidney fibrosis due to an upregulation in Wnt/β-catenin signaling. Here, we demonstrate that KLF15 expression in the kidney was not reduced until later stages of fibrosis in the unilateral uninephrectomy (UUO) murine model. We subsequently investigated the role of KLF15 in fibroblast progenitor cells by generating mice with constitutive loss of *Klf15* in *Foxd1*-expressing cells and subjected these mice to two murine models of fibrosis, UUO and AngII treatment. The loss of *Klf15* in *Foxd1*-expressing cells increased the susceptibility to kidney fibrosis as demonstrated by enhanced extracellular matrix deposition and proliferation of myofibroblasts. Interestingly, downstream targets of Wnt/β-catenin signaling were highly regulated by the level of *Klf15* expression after treatment with Wnt1 ligand. Combined, these data provide strong evidence for the role of KLF15 in kidney fibrosis through regulation of Wnt/β-catenin pathway in myofibroblasts.

RESULTS

KLF15 expression is reduced in late-stage of kidney fibrosis

Since the loss of *Klf15* has been demonstrated to exacerbate fibrosis in other tissues [17, 18], we sought to determine the role of KLF15 in kidney fibrosis. To address this, we initially interrogated the level of Klf15 expression at different stages of kidney fibrosis. We initially performed unilateral ureteral obstruction (UUO) for 3, 7, 10, and 14 days to demonstrate the progression from early to late stage fibrosis as previously reported by other laboratories by masson's trichrome staining (Figure 1A) [19, 20]. Immunostaining and quantification for α-SMA demonstrated an increase in α-SMA expression starting at 3 days post UUO, with a progressive increase at 7 day, 10 day, and 14 days post UUO as compared to sham-treated mice (Figure 1A, 1B). Concurrently, we observed a mild decrease in *Klf15* mRNA expression in total kidney cortex beginning at day 3 post UUO with a more pronounced decrease at day 10 and 14 post UUO as compared to sham-treated mice (Figure 1C). Interestingly, a significant decrease in KLF15 expression by immunostaining was not observed till day 10 and 14 UUO as compared to sham-treated mice (Figure 1A, 1B), suggesting that a decrease in KLF15 is more pronounced at later stages of kidney fibrosis.

Confirmed *Klf15* knockdown in the Foxd1-specific lineage cells

In order to investigate whether the loss of KLF15 exacerbates kidney fibrosis, we sought to knockdown *Klf15* in the kidney. Along with others, we previously demonstrated that KLF15 is ubiquitously expressed in several cell types in the mouse and human kidney (podocytes, mesangial cells, tubular cells, fibroblasts, and endothelial cells) (Figure 1A) [21, 22]. Furthermore, since resident fibroblasts, mesangial cells, and pericytes in the kidney are a major source of kidney fibrosis [23], we initially chose to examine the role of KLF15 specifically in these cells in murine models of kidney fibrosis. The primary source of resident cortical renal fibroblasts, mesangial cells, pericytes, and vascular smooth muscle cells in the kidney are from Forkhead Box D1 (Foxd1) expressing stromal cells in the metanephric mesenchyme during kidney development [24]. *Foxd1* is expressed in the stromal

cells during kidney development, but not in the adult kidney as previously reported [23, 25]. Therefore, we targeted constitutive knockdown of *Klf15* in *Foxd1+* cells using the Cre-loxP recombination system by crossing the *Foxd1-Cre* (C57BL/6) mice with $Klf15^{fl/fl}$ (C57BL/6) mice to generate *Foxd1-Cre* $Klf15^{fl/fl}$ mice (F2). PCR from genomic DNA was used to confirm recombination in the kidney (Supplementary Figure 1A) and isolated primary fibroblasts from *Foxd1-Cre* $Klf15^{+/+}$ and *Foxd1-Cre* $Klf15^{fl/fl}$ mice demonstrates a significant reduction in *Klf15* expression (Supplementary Figure 1B). These findings were confirmed with co-staining for KLF15 with α-SMA in medium sized arteries (Supplementary Figure 1C). *Foxd1-Cre* $Klf15^{fl/fl}$ mice were viable and fertile, similar to that observed in the global $Klf15^{-/-}$ mice [21]. Finally, isolated fibroblasts from six-week-old *Foxd1-Cre* $Klf15^{+/+}$ and *Foxd1-Cre* $Klf15^{fl/fl}$ mice did not demonstrate any significant differences in *Ctgf, Col1α1, Fibronectin*, and *Vimentin* expression (Supplementary Figure 1D).

Klf15 knockdown in the Foxd1-specific lineage cells exacerbates kidney fibrosis post UUO

To determine whether the knockdown of *Klf15* exacerbates renal fibrosis, we initially utilized the UUO model. Since there is typically extensive interstitial fibrosis by 10 and 14 days post UUO (Figure 1A) [19, 20], *Foxd1-Cre* $Klf15^{+/+}$ and *Foxd1-Cre* $Klf15^{fl/fl}$ mice underwent either UUO or sham-treatment for 3 and 7 days to assess whether the loss of *Klf15* in Foxd1 stroma-derived interstitial cells accelerates renal fibrosis at early stages of UUO. Hematoxylin and Eosin (H&E), Periodic Acid-Schiff (PAS), and Masson's Trichrome staining were performed to demonstrate that UUO-treated *Foxd1-Cre* $Klf15^{fl/fl}$ mice exhibited a significant increase in interstitial fibrosis as compared to all other groups at 3 and 7 days post UUO (Figure 2A, 2B). We also observed the kidney weight/body weight was reduced in the UUO-treated *Foxd1-Cre* $Klf15^{fl/fl}$ mice as compared to all other groups (Figure 2C). In addition, we observed an increase in α-SMA and Col1α1 expression in UUO-treated *Foxd1-Cre* $Klf15^{fl/fl}$ mice as compared to all other groups at 3 days post UUO (Figure 3A–C). Finally, UUO-treated *Foxd1-Cre* $Klf15^{fl/fl}$ mice demonstrate an increase in the number of cells with α-SMA with Ki67 expression as compared to all other groups, signifying an increase in the number of myofibroblasts at day 3 post UUO (Figure 3A, D).

To investigate the mechanism by which the loss of *Klf15* in $Foxd1^{+}$ stromal cells accelerates kidney fibrosis, we performed TRANSFAC promoter analysis [26] to identify genes that possess transcriptional binding sites for KLF15. We subsequently performed gene-set enrichment analysis on these genes with KLF15 binding sites using Enrichr [15]. The WikiPathway 2016 gene-set library in Enrichr revealed a significant increase in the pathways involved in the inhibition of the Wnt/β-catenin pathway (Supplementary Table 1).

Since activation of Wnt/β-catenin signaling is critical to the progression of kidney fibrosis and predicted downstream targets of KLF15 are involved in the inhibition of Wnt/β-catenin pathway, we postulated whether the loss of *Klf15* in the UUO model activated Wnt/β-catenin signaling. We observed an increase in the phospho-β-catenin (Ser552) and total β-catenin expression in the UUO-treated *Foxd1-Cre* $Klf15^{fl/fl}$ mice as compared to all other groups at 3 days post UUO (Figure 4B, C, D). Furthermore, UUO-treated *Foxd1-Cre* $Klf15^{fl/fl}$ mice exhibited an increase in c-Myc, a major downstream target of Wnt/β-catenin

signaling involved in progression of kidney fibrosis [6], mRNA and protein expression as compared to all other groups at 3 days post UUO (Figure 4A, B, E).

We subsequently investigated whether the activation in Wnt/β-catenin signaling in the *Foxd1-Cre Klf15*$^{fl/fl}$ mice contributed to a sustained increase in fibrotic markers induced by UUO at 7 days. We observed that key markers involved in kidney fibrosis, *Vimentin, Fibronectin*, and *Col1α1*, were significantly increased in the UUO-treated *Foxd1-Cre Klf15*$^{fl/fl}$ mice as compared to the UUO-treated *Foxd1-Cre Klf15*$^{+/+}$ mice at 7 days (Figure 5A). Similar to 3 days post UUO, we observed an increase in α-SMA and Col1α1 expression in UUO-treated *Foxd1-Cre Klf15*$^{fl/fl}$ mice as compared to the UUO-treated *Foxd1-Cre Klf15*$^{+/+}$ mice by immunostaining (Figure 5B–D). Finally, UUO-treated *Foxd1-Cre Klf15*$^{fl/fl}$ mice also exhibited an increase in α-SMA^{+} and Ki67^{+} cells as compared to UUO-treated *Foxd1-Cre Klf15*$^{+/+}$ mice (Figure 5B, E).

Since studies in cultured fibroblasts have demonstrated that the loss of the *KLF15* contributes to increased extracellular matrix deposition by increasing connective tissue growth factor (CTGF) expression through non-canonical TGFβ signaling [15, 18], we assessed for these changes post-UUO. We observed a significant increase in CTGF expression and Smad2/3 phosphorylation in UUO-treated *Foxd1-Cre Klf15*$^{fl/fl}$ mice as compared to the UUO-treated *Foxd1-Cre Klf15*$^{+/+}$ mice at 7 days (Supplementary Figure 2). Combined, these data suggest that the loss of *Klf15* in Foxd1^{+} stromal cells accelerates kidney fibrosis post UUO, which is potentially linked to concomitant activation of Wnt/β-catenin and TGFβ signaling.

Klf15 knockdown in the Foxd1-specific lineage cells exacerbates Ang II-induced fibrosis

To validate the findings we observed in the UUO model, we utilized the chronic Angiotensin II (AngII) model to investigate whether the loss of *Klf15* in *Foxd1*$^{+}$ stromal cells aggravates kidney fibrosis. Subcutaneous infusion with Ang II for 6 weeks has previously been reported to serve as a viable murine model of kidney fibrosis [27]. Treatment with AngII induced an expected increase in heart weight in both *Foxd1-Cre Klf15*$^{fl/fl}$ and *Foxd1-Cre Klf15*$^{+/+}$ mice (Supplementary Figure 3A). Although AngII treatment contributed to a decrease in kidney weight in both groups, AngII-treated *Foxd1-Cre Klf15*$^{fl/fl}$ exhibited a more pronounced reduction in kidney weight as compared to all other groups (Supplementary Figure 3B). Similarly, we observed a slight, but significant increase in systolic blood pressure (SBP) in AngII-treated *Foxd1-Cre Klf15*$^{fl/fl}$ mice as compared to AngII-treated *Foxd1-Cre Klf15*$^{+/+}$ mice (Supplementary Figure 3C). Furthermore, AngII-treated *Foxd1-Cre Klf15*$^{fl/fl}$ mice exhibited more interstitial fibrosis as compared to all other groups by Masson's Trichrome staining (Figure 6A, 6B). Interestingly, the AngII-treated *Foxd1-Cre Klf15*$^{fl/fl}$ mice also demonstrated an increase in albuminuria, serum urea nitrogen, and creatinine as compared to AngII-treated *Foxd1-Cre Klf15*$^{+/+}$ mice (Figure 6C, 6D, 6E).

Similar to the UUO model, we postulated that the increased renal dysfunction in the AngII-treated *Foxd1-Cre Klf15*$^{fl/fl}$ mice was due to activation in Wnt/β-catenin signaling leading to increased interstitial collagen deposition and fibrosis. The AngII-treated *Foxd1-Cre Klf15*$^{fl/fl}$ mice demonstrated an increase in phospho-β-catenin (Ser552) and total β-catenin as compared to all other groups (Figure 7B–D). Furthermore, c-Myc mRNA and protein

expression was increased in AngII-treated *Foxd1-Cre Klf15*$^{fl/fl}$ mice as compared to all other groups (Figure 7A, B, E). As in the UUO model, immunostaining for α-SMA and Col1α1 was increased in the AngII-treated *Foxd1-Cre Klf15*$^{fl/fl}$ mice as compared to all other groups (Figure 8A–C). Finally, proliferation of myofibroblasts was higher in the AngII-treated *Foxd1-Cre Klf15*$^{fl/fl}$ mice as compared to the AngII-treated *Foxd1-Cre Klf15*$^{+/+}$ mice (Figure 8D). Together, these data suggest that the loss of *Klf15* in Foxd1^{+} stromal cells increases the susceptibility to Ang II-induced kidney fibrosis, which might be secondary to activation of Wnt/β-catenin signaling.

Increase in fibrotic markers and renal dysfunction in older *Foxd1-Cre Klf15*$^{fl/fl}$ mice

To ascertain whether the loss of *Klf15* in *Foxd1*$^{+}$ stromal cells increases the susceptibility to fibrosis and renal dysfunction, we aged *Foxd1-Cre Klf15*$^{+/+}$ and *Foxd1-Cre Klf15*$^{fl/fl}$ mice for 52 weeks. These older *Foxd1-Cre Klf15*$^{fl/fl}$ mice revealed an increase in interstitial inflammation and fibrosis as compared to age-matched *Foxd1-Cre Klf15*$^{+/+}$ mice by H&E and PAS staining (Figure 9A). Furthermore, α-SMA and Col1α1 expression was higher in the *Foxd1-Cre Klf15*$^{fl/fl}$ mice as compared to *Foxd1-Cre Klf15*$^{+/+}$ mice (Figure 9A–B). Finally, these age-matched *Foxd1-Cre Klf15*$^{fl/fl}$ mice demonstrated a mild, yet significant increase in serum urea nitrogen and creatinine as compared to *Foxd1-Cre Klf15*$^{+/+}$ mice (Figure 9C–D). These data suggest that the loss of *Klf15* in *Foxd1*$^{+}$ stromal cells increases the susceptibility to fibrosis and renal dysfunction in aging mice.

Expression of *Klf15* modulates Wnt/β-catenin signaling

To investigate the role of KLF15 in regulating Wnt/β-catenin signaling, we initially generated mouse embryonic fibroblasts (MEFs) with stable knockdown for *Klf15.* Knockdown for *Klf15* (*Klf15-shRNA*) in MEFs was confirmed by western blot (Supplementary Figure 4A). We also generated Wnt1 ligand by collecting the supernatant from human embryonic kidney (HEK293) cells overexpressing *Wnt1*. Confirmation of Wnt1 ligand in the supernatant is demonstrated by western blot (Supplementary Figure 4B). Subsequently, *Klf15-shRNA* and *EV-shRNA* (control) MEFs were treated with Wnt1 ligand for 48 hours to assess for changes in expression of Wnt/β-catenin downstream targets and fibrotic markers. Wnt1-treated *Klf15-shRNA* MEFs exhibited a significant increase in *Col1α1* and *Fibronectin* expression as compared to all other groups (Figure 10A). Furthermore, we observed a significant increase in c-Myc expression in Wnt1-treated *Klf15-shRNA* MEFs as compared to all other groups (Figure 10A, 10B). Since activation of Wnt/β-catenin signaling contributes to cell proliferation and we observed an increase in proliferating myofibroblasts in the UUO and AngII murine models (Figures 3, 5, 8), we assessed for changes in cell proliferation in MEFs after Wnt1 treatment. Wnt1-treated *Klf15-shRNA* MEFs demonstrated increased proliferation as compared to Wnt1-treated *EV-shRNA* MEFs (Figure 10C). To validate that the loss of *Klf15* in MEFs activates Wnt/β-catenin signaling, we treated *Klf15-shRNA* and *EV-shRNA* MEFs with commercially available Wnt1 ligand (120–17; PeproTech) at variable concentrations for 48 hours. We observed that phospho-β-catenin, total-β-catenin, and c-Myc expression were increased in *Klf15-shRNA* MEFs as compared to *EV-shRNA* MEFs at increasing concentration of Wnt1 ligand (Supplementary Figure 4C). Conversely, we overexpressed V5-tagged *KLF15* (*lentiORF-KLF15*) in Wnt1 expressing (*pNL-Wnt1*) HEK293 cells to determine whether the

induction in *KLF15* inhibited Wnt/β-catenin signaling. We initially confirmed overexpression of KLF15 in HEK293 cells by Western blot (Figure 10D). *LentiORF-KLF15* cells exhibited a significant reduction in phospho-β-catenin (Ser552) with no significant changes in total β-catenin expression as compared to control (*lentiORF-RFP*) cells (Figure 10D). Since there were no significant changes in total β-catenin expression with *KLF15* overexpression, we sought to determine whether KLF15 suppressed transcriptional activity of β-catenin by binding and inhibiting its phosphorylation as previously described [16]. To validate this interaction, we initially immunoprecipitated KLF15 with both anti-V5 and anti-KLF15 antibody and subsequently detected β-catenin with anti-β-catenin antibody to demonstrate the enhanced binding of KLF15 to β-catenin in Wnt1 expressing cells (Figure 10E). Combined, these data suggest that changes in KLF15 expression mediate canonical Wnt signaling under profibrotic stimuli.

KLF15 expression is reduced in human biopsies with kidney fibrosis

To ascertain the role of KLF15 in kidney fibrosis, we initially examined previously reported gene expression arrays from kidney biopsy specimens with arterial hypertension and diabetic kidney disease (DKD) as compared to healthy donor nephrectomies [28, 29]. Since KLF15 is expressed in the glomerular compartment as well as the tubulointerstitial compartment [21, 22], we specifically measured KLF15 expression in RNA extracted from laser capture microdissected tubulointerstitial kidney biopsies with arterial hypertension and DKD as compared to healthy donor subjects [28, 29] (Figure 11A, 11B). To further validate these findings, we measured KLF15 and α-SMA expression by immunostaining de-identified kidney biopsies with early and late-stage DKD as compared to healthy donor subjects. We observed a significant reduction in KLF15 expression in early and late-stage DKD as compared to healthy donor subjects (Figure 11C, 11D). Collectively, with the rest of our findings, these data suggest that the loss of KLF15 is critical to the progression of human kidney fibrosis.

DISCUSSION

Several studies have clearly demonstrated that along with severity of epithelial injury, repeated insults to the tubular epithelium lead to eventual fibrosis of the kidney. Along with circulating factors, paracrine signaling between the tubular epithelium and the renal stromal cells play a vital role in the development and progression of fibrosis. However, the signals in the recipient stromal progenitor cells that drive myofibroblast differentiation and proliferation are unclear. In this study, we report that the loss of *Klf15* in *Foxd1*$^{+}$ stromal cells increases the susceptibility to kidney fibrosis due to activation of Wnt/β-catenin signaling. The following findings support this conclusion: 1) KLF15 expression in the kidney is reduced more significantly in later stages of fibrosis in the UUO model, 2) Foxd1-specific knockdown of *Klf15* increased ECM deposition and myofibroblast proliferation, phospho-β-catenin (Ser552), and c-Myc expression in two murine models of fibrosis, 3) Knockdown of *Klf15* in cultured MEFs also enhanced Wnt/β-catenin signaling after treatment with Wnt1 ligand, 4) Overexpression of *KLF15* in Wnt1 expressing cells attenuated Wnt/β-catenin signaling, and 5) KLF15 expression is reduced in the

tubulointerstitial compartment of kidney biopsies with fibrosis as compared to healthy donor subjects.

Molecules that mediate the myofibroblast differentiation and proliferation in renal stromal cells under cell stress are largely undefined. Although secretion of Wnt ligands from the injured tubular epithelium can trigger myofibroblast differentiation and proliferation, transcription regulators that retard this process in the stromal progenitor cells are unclear. Although, we observed a decrease in *Klf15* mRNA expression within 3 days post-UUO, significant decreases in KLF15 protein expression were not observed till later stages of fibrosis. We hypothesize an initial reno-protective response of KLF15 in early post-UUO to prevent significant myofibroblast activation and proliferation, which is lost at late stages of fibrosis. To test this hypothesis, we initially utilized the *Foxd1-Cre* mice to knockdown *Klf15* in renal stromal cells to determine that *Klf15* is vital in attenuating the progression of kidney fibrosis under cell stress. Although previous studies have reported that the global loss of *Klf15* exacerbates kidney and cardiac fibrosis [14, 17], cell-specific role of KLF15 in renal fibrosis remains unclear. To date, this is the first study to utilize the renal stromal progenitor-specific knockdown of *Klf15* and confirm a critical role of KLF15 in the regulation of myofibroblast proliferation. Since KLF15 is also expressed in other cell types in the kidney[22], the effects of KLF15 expression in non-stromal cells cannot be neglected. As such, future studies will need to focus on investigating whether changes in KLF15 expression in other kidney cells (i.e. tubular cells, endothelial cells) can modulate the release of paracrine factors that stimulate myofibroblast differentiation and proliferation.

Mice homozygous for the knockin allele results in embryonic lethality since it affects Foxd1 function during development [30–32]. Therefore, *Foxd1-Cre* mice are heterozygous for the knockin allele [32], and consequently only exhibit partial knockdown in *Klf15* expression. We believe that complete knockout of *Klf15* may induce more severe interstitial fibrosis observed in the UUO and AngII-treated *Foxd1-Cre Klf15*$^{fl/fl}$ mice. In our future studies we will need to utilize Crispr/Cas9 technology to generate mice with complete Foxd1-specific deletion of *Klf15* to ascertain whether *Klf15* plays an essential role in the activation of myofibroblasts in kidney fibrosis.

Our data suggests that the loss of *Klf15* in *Foxd1+* stromal cells induces myofibroblast proliferation due to activation of Wnt/β-catenin signaling. Although activation of canonical Wnt/β-catenin signaling contributes to myofibroblast activation, it is likely not the sole pathway. Recent studies demonstrate concomitant activation of TGFβ and Wnt signaling synergistically increased profibrotic genes and accelerated interstitial fibrosis [5]. In addition, transcriptional cooperation of TGFβ and Wnt pathways resulted in differential expression of key transcripts such as connective tissue growth factor (CTGF) expression. Interestingly, studies in cardiac fibroblasts demonstrated that KLF15 is a negative regulator of connective tissue growth factor (CTGF) expression [18]. Similarly, we observed increased activation of the TGFβ pathway with increased CTGF expression in *Foxd1-Cre Klf15*$^{fl/fl}$ mice as compared to *Foxd1-Cre Klf15*$^{+/+}$ mice post-UUO. Consequently, we will need to ascertain the mechanism by which the loss of *Klf15* in *Foxd1+* cells also contributes to concomitant activation of TGFβ and Wnt/β-catenin signaling.

Based on these data, we hypothesize that the induction of *KLF15* will attenuate myofibroblast activation and eventual fibrosis. We observed that overexpression of *KLF15* in Wnt1 expressing cells attenuated Wnt/β-catenin signaling. Recent studies in cardiac progenitor cells show that KLF15 binds to β-catenin and enhances its proteosomal degradation, thereby inhibiting the transcriptional activity of β-catenin [16]. Similarly, our current studies suggest that induction of *KLF15* suppresses Wnt/β-catenin signaling by binding and inhibiting the phosphorylation of active β-catenin. To further confirm the anti-fibrotic effects of KLF15, we also need to determine whether induction of renal resident fibroblast-specific induction of *KLF15* expression in mice suppresses the transcriptional activity of β-catenin and attenuates renal fibrosis.

To the best of our knowledge, this is the first study to demonstrate a novel transcriptional mediator of Wnt-mediated myofibroblast activation in kidney fibrosis. Specifically, our studies suggest that the loss of KLF15 activated Wnt/β-catenin pathway, myofibroblast activation and proliferation, and increased ECM deposition under profibrotic stimuli in the kidney. Collectively, these findings suggest that KLF15 could be considered as a potential drug target for anti-fibrosis therapy in kidney disease.

CONCISE METHODS

Genotyping of Foxd1-Cre-GFP Klf15$^{fl/fl}$ mice

Klf15$^{fl/fl}$ (C57BL/6) mice were generated by inserting LoxP sites flanking exon 2 of the *Klf15* gene as previously reported [33]. *Klf15*$^{fl/fl}$ mice (C57BL/6) were crossed with mice expressing *Cre* recombinase under the control of the *Foxd1* promoter (B6; 129S4-Foxd1<tm1 (GFP/cre)Amc>/J; Jackson Laboratory). After two generations of breeding, *Foxd1-Cre Klf15*$^{fl/fl}$ and *Foxd1-Cre Klf15*$^{+/+}$ (control) mice were used in the experimental groups. Genotyping by tail preparation and PCR were performed at two weeks of age as previously described [21].

Unilateral ureteric obstruction (UUO) model

In the UUO model, 12-week old *Foxd1-Cre Klf15*$^{fl/fl}$ and *Foxd1-Cre Klf15*$^{+/+}$ littermates either underwent sham or UUO as previously reported [6, 34]. Briefly, a small incision was made through the left flank muscle, and the left kidney was exteriorized. 4-0 silk suture was used to tie the surgical knot around the left ureter at the bottom of left kidney. Sham-treated and UUO-treated mice were sacrificed at either day 3 or 7 UUO and both kidneys (obstructed and contralateral) were harvested for RNA, protein, and histopathology.

Angiotensin II (AngII) murine model

Ang II was continuously infused via subcutaneous route as previously reported [27]. Briefly, AngII or vehicle was infused at a continuous rate of 2.5 μg/kg/min from a subcutaneous insertion of osmotic mini pump (Alzet 2006) for 6 weeks in male *Foxd1-Cre Klf15*$^{fl/fl}$ and *Foxd1-Cre Klf15*$^{+/+}$ mice. At 6 weeks, mice underwent systolic blood pressure measurements with tail-cuff manometry and mice were subsequently sacrificed.

Measurement of serum urea nitrogen and creatinine

Serum urea nitrogen was measured by colorimetric detection method (Arbor Assays) as per manufacturer's protocol. Serum creatinine was measured by the Isotope Dilution LC-MS/MS at the University of Alabama at Birmingham O'Brien Core Center.

Measurement of systolic blood pressure

Systolic blood pressure was measured by CODA noninvasive tail-cuff sphygmomanometer (Kent Scientific, Charlotte, NC) on conscious mice after 6 weeks of AngII infusion as previously reported [35]. Prior to blood pressure measurements, mice were initially subjected to acclimation period of five cycles before blood pressure assessment. After the acclimation period, blood pressure was measured in each mouse for 60 continuous cycles and an average was quantified [35].

Cell culture

Immortalized mouse embryonic fibroblast (MEF) cells were grown in DMEM with 10% FBS. MEFs were seeded in six-well plates at the confluence of 60%–70%, serum starved for 24 hours, and subsequently treated with Wnt1 ligand (supernatant collected from pNL-CMVWnt1IRESEGFP-WPREΔU3 (*pNL-Wnt1*) cells) or vehicle (supernatant collected from pNL-CMVIRESEGFP-WPREΔU3 (*pNL-GFP*) cells) for 48 hours. Subsequently, cells were harvested for real-time PCR, western blot, and MTT assay.

MEFs were also treated with vehicle or Wnt1 ligand (120–17; PeproTech) at 0.25, 0.5, 1.0 μg/ml for 48 hours. Subsequently, cells were harvested for western blot.

shRNA-mediated Klf15 knockdown using lentivirus

Klf15 knockdown in MEFs was performed using Genecopoeia lentiviral shRNAmir system with MSH032956-1-LVRU6GP (*shRNA-Klf15*) and CSHCTR001-LVRU6GP (*shRNA-EV*) constructs. In brief, lentiviral particles were produced by transfecting HEK293 cells with a combination of lentiviral expression plasmid DNA, pCD/NL-BH ΔΔΔ packaging plasmid, and VSV-G-encoding pLTR-G plasmid. For cell infection, viral supernatants were supplemented with 8μg/ml polybrene and incubated with cells for a 24-hour period. Cells expressing shRNA were selected with 1.25μg/ml puromycin for 2–3 weeks prior to use in all studies. Western blot were performed to confirm *Klf15* knockdown.

Western blot analysis

Tissue or cell lysates were lysed with laemmli buffer containing 1% Triton, a protease inhibitor cocktail, and tyrosine and serine-threonine phosphorylation inhibitors. Lysates were subjected to immunoblot analysis using rabbit anti-V5 (ab15828; Abcam), rabbit anti-KLF15 (ABC471; Millipore), rabbit anti-GAPDH (MAB374; Millipore), rabbit anti-total Smad2/3 (3102S, Cell Signaling Technology), rabbit anti-phospho Smad2/3 (8828S, Cell Signaling Technology), mouse anti-α-SMA (A5228; Sigma), mouse anti-total β-catenin (BD610153), rabbit anti-phospho-β-catenin (ser552) (9566; Cell Signaling Technology), rabbit anti-c-Myc (5605s; Cell Signaling Technology), and rabbit anti-Wnt1 (365800; Invitrogen) as previously reported [36].

LentiORF-*KLF15* overexpression and co-immunoprecipitation

V5-tagged LentiORF-*KLF15* clone was purchased from Genecopoeia and transient *KLF15* overexpression was achieved by transfecting *pNL-Wnt1 and pNL-GFP* HEK293 cells using Viafect (Promega). Western blot for V5 and KLF15 were performed to confirm *KLF15* overexpression in lentiORF-*KLF15* as compared to lentiORF-*RFP* cells. Cells were harvested 48 hours after transfection and lysed with radio-immunoprecipitation assay (RIPA) buffer with protease inhibitors, and immunoprecipitated with antibodies against rabbit anti-V5 antibody and rabbit anti-KLF15 antibody. Interacting β-catenin was detected by immunoblotting with rabbit anti-β-catenin antibody. As controls, protein lysates transfected with control vector (LentiORF-RFP) and precipitation with IgG isotype control were used for each group. Input (2%) of whole cell lysates was immunoblotted with total β-catenin and GAPDH to detect protein expression as previously reported [16].

Real-time PCR

Total RNA was extracted by using TRIzol (GIBCO Life Technology). First-strand cDNA was prepared from total RNA (1.5 μg) using the SuperScript® VILO cDNA Synthesis Kit and Master Mix (Thermo Fisher Technologies), and cDNA (1 μl) was amplified in triplicate using SYBR GreenER qPCR Supermix on an ABI Quantstudio® 3 Real-Time PCR instrument (Applied Biosystems). Primers for mouse *Klf15*, mouse *Col1α1*, mouse *Vimentin*, mouse *Fibronectin*, mouse *c-Myc*, and mouse *Ctgf* were designed using NCBI/Primer-BLAST (Supplemental Table 2). Light cycler analysis software was used to determine crossing points using the second derivative method. Data were normalized to housekeeping genes (*ACTB*) and presented as fold increase compared with RNA isolated from the control group using the $2^{-\Delta\Delta CT}$ method.

Cell proliferation

MEF cell lines with shRNA of scramble DNA and *Klf15* were seeded at the concentration of $2X10^4$ cells/ml in a 96 well plate, serum starved for 24 hours and treated with Wnt1 ligand or vehicle for 48 hours. 3-(4, 5-dimethylthiazolyl-2)-2, 5-diphenyltetrazolium bromide (MTT) assay (Promega G3582) was used to measure the proliferation of the cells. Briefly, 20μl of Cell Titer 96 Aqueous One Solution Reagent was added to each well. After incubation at 37C for 4 hours, the absorbance at 490nm was recorded by using a 96-well plate reader SpectraMax M3 (Molecular Devices).

Histopathology by bright-field light microscopy

Mice were perfused with HBSS, and the kidneys were fixed in 10% phosphate-buffered formalin overnight and switched to 70% ethanol before processing for histology. Kidney tissues were embedded in paraffin by American Histolabs, and 3-μm-thick sections were stained with Periodic Acid–Schiff (PAS) (Sigma-Aldrich), Hematoxylin and Eosin (H&E), and Masson's Trichrome staining. Quantification of fold change in percent area stained with Masson's Trichrome was determined using ImageJ 1.26t software (National Institute of Health, rsb.info.nih.gov/ij).

Immunofluorescence

Immunofluorescence was performed as recently reported [22]. In brief, blank slides were initially baked overnight at 55–60°C and were then processed as pre viously described. Formalin-fixed and paraffin-embedded sections were deparaffinized, and endogenous peroxidase was inactivated with H_2O_2. After blocking, sections were incubated with a rabbit anti-Col1α1 antibody (SC-7158; Santa Cruz Biotechnology Inc.), a mouse anti-α-SMA antibody (A5228, Sigma), a rabbit anti-Ki67 antibody (Biocare Medical), and a rabbit anti-KLF15 (Genscript) at 4°C overnight. Subsequent ly, slides were washed and sections were incubated with a fluorophore-linked secondary antibody. After staining, slides were mounted in Prolong gold antifade mounting media (Invitrogen P36930) and photographed under a Nikon Eclipse i90 microscope with a digital camera. Quantification of intensity and cell number was performed using ImageJ 1.26t software. De-identified human biopsy specimens were acquired from Stony Brook University School of Medicine. Early (<10%) and late (>50%) chronic tubulointerstitial fibrosis was determined by the renal pathologist (MPR) based on the percentage of affected cortical area. Subsequently, immunostaining for KLF15 and α-SMA was performed with quantification of fold change in intensity of KLF15 expression and percent area of α-SMA was determined using ImageJ 1.26t software.

Isolation of primary mouse fibroblasts

Primary mouse fibroblasts were isolated from kidneys of *Foxd1-Cre Klf15*$^{fl/fl}$ and *Foxd1-Cre Klf15*$^{+/+}$ mice as previously reported [34, 37]. Briefly, after HBSS perfusion of anesthetized mice [38], the kidneys were cut into 1 mm^3 sections, seeded in 10 cm plates coated with Type I collagen, and grown in high glucose DMEM with 20% FBS. After cell outgrowth from the explants, the remaining tissue was discarded. Cells were split at a 1:5 ratio after confluency was reached. After 1–2 passages, the cells were harvested in TRIzol and the *Klf15* expression level was measured by real-time pcr. The specificity of primary fibroblast isolation was determined by measuring the expression for fibroblast (α-SMA and Vimentin) markers as previously reported [37].

Promoter analysis

As previously reported, using the TRANSFAC software [26] we scanned the promoters of all mouse genes in the region from (−2000) to the transcription start site with the KLF15 position weight matrix provided by the TRANSFAC system [22]. Enrichment analysis was performed using Enrichr and the Fisher's Exact test was used to determine the terms that were overrepresented among the genes with KLF15 binding sites [39].

Statistical Analysis

All data will be assessed for normality, and then parametric or non-parametric tests were employed for data analysis, as appropriate. The unpaired two-tailed t test was used to compare data between two groups and one-way ANOVA with Tukey's post-hoc test to compare data between more than two groups. For data sets that we could not assume normality, nonparametric statistical tests were performed using the Mann-Whitney test to compare data between the two groups and the Kruskal-Wallis test with Dunn's post-hoc test to compare data between more than two groups. The exact test used for each experiment is

noted in the figure legends. Data are expressed as mean ± SEM (X ± SEM). All experiments were repeated a minimum of three times, and representative experiments are shown. Statistical significance was considered when $p < 0.05$. All statistical analysis was performed using GraphPad Prism 6.0a.

Study approval

All animal studies conducted were approved by the Stony Brook University Animal Institute Committee approved all animal studies. NIH Guide for the Care and Use of Laboratory Animals was followed strictly. Stony Brook University Institutional Review Board approved the use of archived de-identified human biopsy specimens for immunostaining.

Supplementary Material

Refer to Web version on PubMed Central for supplementary material.

Acknowledgments

This work was supported by funds from the NIH/NIDDK (DK102519 to SKM, DK078897, DK088541, and DK56492 to JH), National Natural Science Foundation of China (81100526 to XG), Shanghai Municipal Natural Science Foundation (14ZR1442200 to XG), and Shanghai Top Priority Key Clinical Disciplines Construction Project to CM.

References

1. Geng H, Lan R, Wang G, et al. Inhibition of autoregulated TGFbeta signaling simultaneously enhances proliferation and differentiation of kidney epithelium and promotes repair following renal ischemia. Am J Pathol. 2009; 174:1291–1308. [PubMed: 19342372]
2. Campanholle G, Ligresti G, Gharib SA, et al. Cellular mechanisms of tissue fibrosis. 3. Novel mechanisms of kidney fibrosis. Am J Physiol Cell Physiol. 2013; 304:C591–603. [PubMed: 23325411]
3. Venkatachalam MA, Griffin KA, Lan R, et al. Acute kidney injury: a springboard for progression in chronic kidney disease. Am J Physiol Renal Physiol. 2010; 298:F1078–1094. [PubMed: 20200097]
4. Duffield JS. Cellular and molecular mechanisms in kidney fibrosis. J Clin Invest. 2014; 124:2299–2306. [PubMed: 24892703]
5. Maarouf OH, Aravamudhan A, Rangarajan D, et al. Paracrine Wnt1 Drives Interstitial Fibrosis without Inflammation by Tubulointerstitial Cross-Talk. J Am Soc Nephrol. 2016; 27:781–790. [PubMed: 26204899]
6. He W, Dai C, Li Y, et al. Wnt/beta-catenin signaling promotes renal interstitial fibrosis. J Am Soc Nephrol. 2009; 20:765–776. [PubMed: 19297557]
7. Maarouf OH, Ikeda Y, Humphreys BD. Wnt signaling in kidney tubulointerstitium during disease. Histol Histopathol. 2015; 30:163–171. [PubMed: 25297005]
8. Carroll TJ, Park JS, Hayashi S, et al. Wnt9b plays a central role in the regulation of mesenchymal to epithelial transitions underlying organogenesis of the mammalian urogenital system. Dev Cell. 2005; 9:283–292. [PubMed: 16054034]
9. Li VS, Ng SS, Boersema PJ, et al. Wnt signaling through inhibition of beta-catenin degradation in an intact Axin1 complex. Cell. 2012; 149:1245–1256. [PubMed: 22682247]
10. Clevers H, Nusse R. Wnt/beta-catenin signaling and disease. Cell. 2012; 149:1192–1205. [PubMed: 22682243]
11. McConnell BB, Yang VW. Mammalian Kruppel-like factors in health and diseases. Physiol Rev. 2010; 90:1337–1381. [PubMed: 20959618]
12. Mallipattu SK, Estrada CC, He JC. The critical role of Kruppel-like factors in kidney disease. Am J Physiol Renal Physiol. 2017; 312:F259–F265. [PubMed: 27852611]

13. Bialkowska AB, Yang VW, Mallipattu SK. Kruppel-like factors in mammalian stem cells and development. Development. 2017; 144:737–754. [PubMed: 28246209]
14. Gao X, Huang L, Grosjean F, et al. Low-protein diet supplemented with ketoacids reduces the severity of renal disease in 5/6 nephrectomized rats: a role for KLF15. Kidney Int. 2011; 79:987–996. [PubMed: 21248717]
15. Gao X, Wu G, Gu X, et al. Kruppel-like factor 15 modulates renal interstitial fibrosis by ERK/MAPK and JNK/MAPK pathways regulation. Kidney Blood Press Res. 2013; 37:631–640. [PubMed: 24356553]
16. Noack C, Zafiriou MP, Schaeffer HJ, et al. Krueppel-like factor 15 regulates Wnt/beta-catenin transcription and controls cardiac progenitor cell fate in the postnatal heart. EMBO Mol Med. 2012; 4:992–1007. [PubMed: 22767436]
17. Fisch S, Gray S, Heymans S, et al. Kruppel-like factor 15 is a regulator of cardiomyocyte hypertrophy. Proc Natl Acad Sci U S A. 2007; 104:7074–7079. [PubMed: 17438289]
18. Wang B, Haldar SM, Lu Y, et al. The Kruppel-like factor KLF15 inhibits connective tissue growth factor (CTGF) expression in cardiac fibroblasts. J Mol Cell Cardiol. 2008; 45:193–197. [PubMed: 18586263]
19. Klahr S, Morrissey J. Obstructive nephropathy and renal fibrosis. Am J Physiol Renal Physiol. 2002; 283:F861–875. [PubMed: 12372761]
20. Chevalier RL, Forbes MS, Thornhill BA. Ureteral obstruction as a model of renal interstitial fibrosis and obstructive nephropathy. Kidney Int. 2009; 75:1145–1152. [PubMed: 19340094]
21. Mallipattu SK, Liu R, Zheng F, et al. Kruppel-Like factor 15 (KLF15) is a key regulator of podocyte differentiation. J Biol Chem. 2012
22. Mallipattu SK, Guo Y, Revelo MP, et al. Kruppel-Like Factor 15 Mediates Glucocorticoid-Induced Restoration of Podocyte Differentiation Markers. J Am Soc Nephrol. 2016
23. Humphreys BD, Lin SL, Kobayashi A, et al. Fate tracing reveals the pericyte and not epithelial origin of myofibroblasts in kidney fibrosis. Am J Pathol. 2010; 176:85–97. [PubMed: 20008127]
24. Gomez IG, Duffield JS. The FOXD1 lineage of kidney perivascular cells and myofibroblasts: functions and responses to injury. Kidney Int Suppl (2011). 2014; 4:26–33. [PubMed: 26312147]
25. Kobayashi H, Liu Q, Binns TC, et al. Distinct subpopulations of FOXD1 stroma-derived cells regulate renal erythropoietin. J Clin Invest. 2016; 126:1926–1938. [PubMed: 27088801]
26. Matys V, Fricke E, Geffers R, et al. TRANSFAC: transcriptional regulation, from patterns to profiles. Nucleic Acids Res. 2003; 31:374–378. [PubMed: 12520026]
27. Fraune C, Lange S, Krebs C, et al. AT1 antagonism and renin inhibition in mice: pivotal role of targeting angiotensin II in chronic kidney disease. Am J Physiol Renal Physiol. 2012; 303:F1037–1048. [PubMed: 22791343]
28. Woroniecka KI, Park AS, Mohtat D, et al. Transcriptome analysis of human diabetic kidney disease. Diabetes. 2011; 60:2354–2369. [PubMed: 21752957]
29. Ju W, Nair V, Smith S, et al. Tissue transcriptome-driven identification of epidermal growth factor as a chronic kidney disease biomarker. Sci Transl Med. 2015; 7:316ra193.
30. Hatini V, Huh SO, Herzlinger D, et al. Essential role of stromal mesenchyme in kidney morphogenesis revealed by targeted disruption of Winged Helix transcription factor BF-2. Genes Dev. 1996; 10:1467–1478. [PubMed: 8666231]
31. Levinson R, Mendelsohn C. Stromal progenitors are important for patterning epithelial and mesenchymal cell types in the embryonic kidney. Semin Cell Dev Biol. 2003; 14:225–231. [PubMed: 14627121]
32. Kobayashi A, Mugford JW, Krautzberger AM, et al. Identification of a multipotent self-renewing stromal progenitor population during mammalian kidney organogenesis. Stem Cell Reports. 2014; 3:650–662. [PubMed: 25358792]
33. Lu Y, Zhang L, Liao X, et al. Kruppel-like factor 15 is critical for vascular inflammation. J Clin Invest. 2013; 123:4232–4241. [PubMed: 23999430]
34. Ma FY, Tesch GH, Nikolic-Paterson DJ. ASK1/p38 signaling in renal tubular epithelial cells promotes renal fibrosis in the mouse obstructed kidney. Am J Physiol Renal Physiol. 2014; 307:F1263–1273. [PubMed: 25298527]

35. Mallipattu SK, Gallagher EJ, LeRoith D, et al. Diabetic nephropathy in a nonobese mouse model of type 2 diabetes mellitus. Am J Physiol Renal Physiol. 2014; 306:F1008–1017. [PubMed: 24598803]

36. Mallipattu SK, Horne SJ, D'Agati V, et al. Kruppel-like factor 6 regulates mitochondrial function in the kidney. J Clin Invest. 2015; 125:1347–1361. [PubMed: 25689250]

37. Delle H, Rocha JR, Cavaglieri RC, et al. Antifibrotic effect of tamoxifen in a model of progressive renal disease. J Am Soc Nephrol. 2012; 23:37–48. [PubMed: 22052053]

38. Mallipattu SK, Liu R, Zhong Y, et al. Expression of HIV transgene aggravates kidney injury in diabetic mice. Kidney Int. 2013; 83:626–634. [PubMed: 23325078]

39. Chen EY, Tan CM, Kou Y, et al. Enrichr: interactive and collaborative HTML5 gene list enrichment analysis tool. BMC Bioinformatics. 2013; 14:128. [PubMed: 23586463]

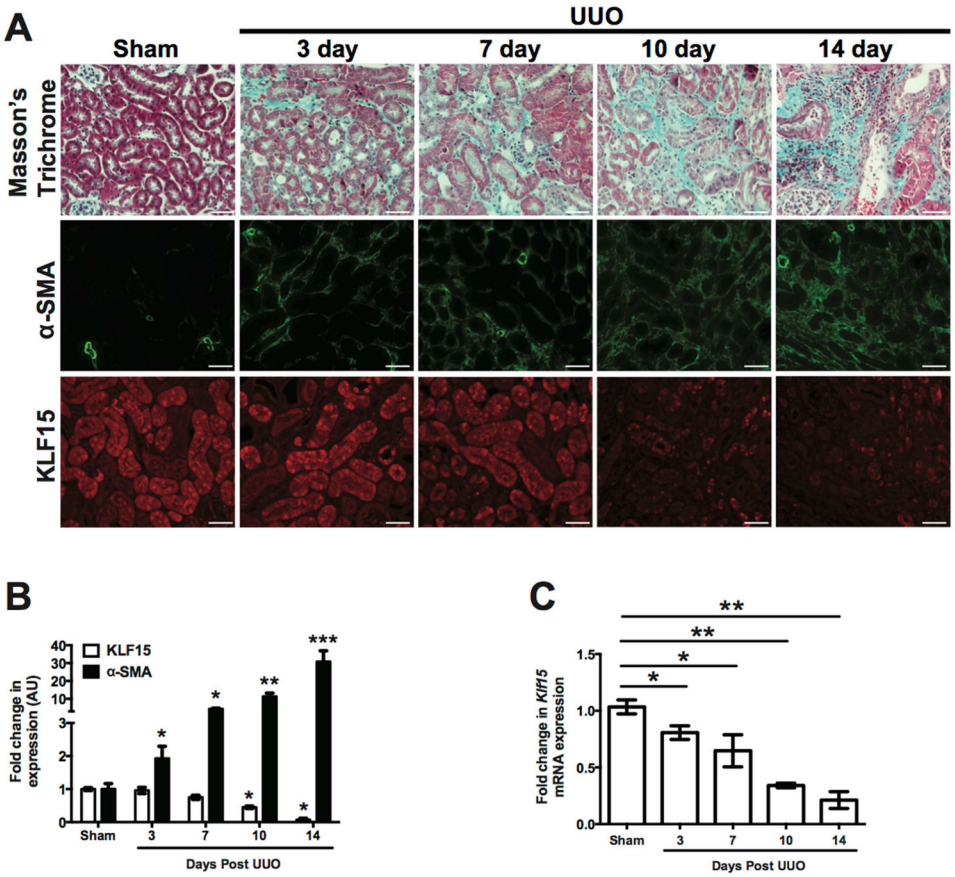

Figure 1. KLF15 expression is reduced in later stages of UUO

Wildtype mice underwent UUO or sham treatment for 3, 7, 10, and 14 days. **(A)** Masson's Trichrome and immunostaining for α-SMA and KLF15 staining were performed. The representative images of six independent experiments are shown in the top panel (X 20). **(B)** Quantification of immunostaining for α-SMA and KLF15. **(C)** RNA was extracted from total kidney cortex and RT-PCR was performed for *Klf15* expression (n=6, *p<0.05, **p<0.01, ***p<0.001, Mann-Whitney test).

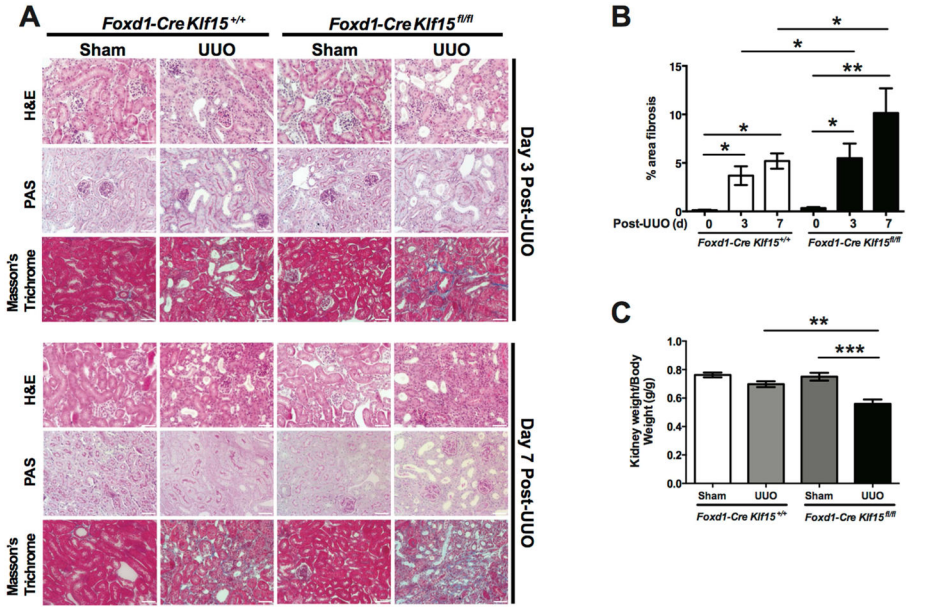

Figure 2. Loss of *Klf15* in Foxd1+ stromal cells exacerbates fibrosis in UUO model

Age-matched 12-week-old *Foxd1-Cre Klf15$^{fl/fl}$* and *Foxd1-Cre Klf15$^{+/+}$* mice were concurrently treated with UUO or sham for 3 and 7 days. **(A)** All mice were sacrificed and renal cortex fixed for histology. Hematoxylin and Eosin (H&E), Periodic acid-Schiff (PAS), and Masson's Trichrome staining was performed to evaluate for tubulointerstitial changes. The representative images from 4 mice in each group are shown (X 20). **(B)** % area fibrosis from Masson's Trichrome stain is shown. **(C)** Kidney weight/body weight was measured at 7 days post UUO or sham treatment (n=6, *p<0.01, **p<0.01, ***p<0.001, One-way ANOVA test with Tukey's post-test).

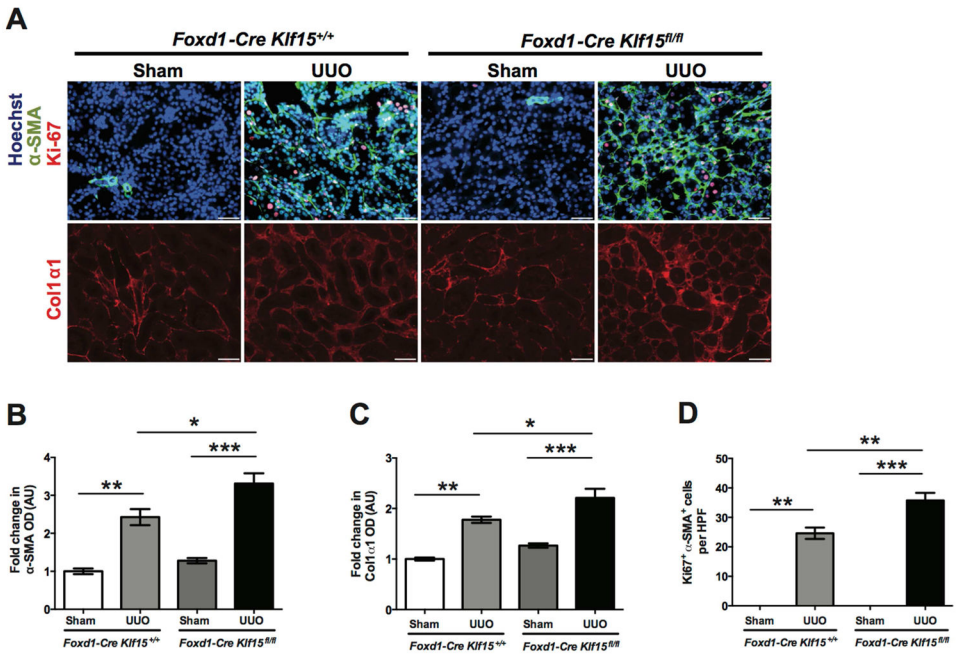

Figure 3. Loss of *Klf15* in Foxd1+ stromal cells increases the expression of fibrotic markers 3 days post UUO

Age-matched 12-week-old *Foxd1-Cre Klf15$^{fl/fl}$* and *Foxd1-Cre Klf15$^{+/+}$* mice were concurrently treated with UUO or sham for 3 days. **(A)** Immunostaining for α-SMA and Ki67 (top panel) and Col1α1 (bottom panel) was performed in all groups of mice. Representative images from four mice in each group are shown (X 20). ImageJ was used to quantify the area stained per high power field (HPF) as a relative fold change to sham-treated *Foxd1-Cre Klf15$^{+/+}$* mice for **(B)** α-SMA and **(C)** Col1α1. **(D)** Quantification of myofibroblast proliferation was determined by quantifying the number of Ki67+ and α-SMA+ cells per HPF. (n=6, *p<0.05, **p<0.01, ***p<0.001, Kruskal-Wallis test with Dunn's post-test).

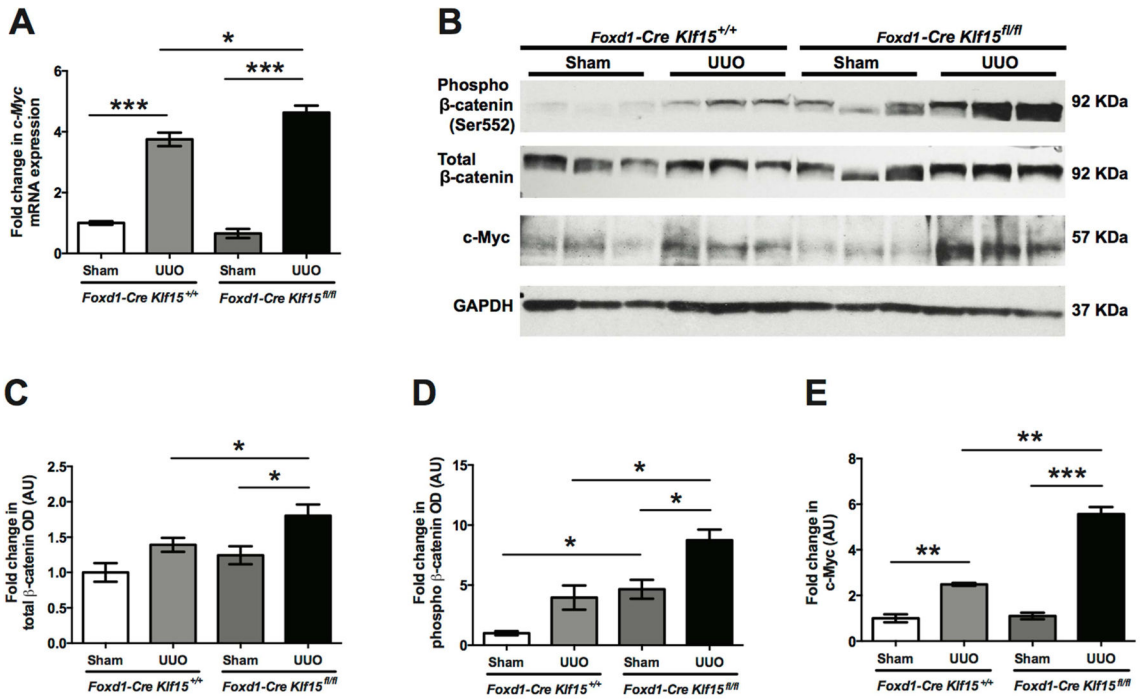

Figure 4. Activation of Wnt/β-catenin signaling in UUO-treated *Foxd1-Cre Klf15$^{fl/fl}$* mice

(A) RNA was extracted from total kidney cortex and RT-PCR was performed for *c-Myc* expression from 12-week-old *Foxd1-Cre Klf15$^{fl/fl}$* and *Foxd1-Cre Klf15$^{+/+}$* mice treated with sham or UUO for 3 days. (n=6, *p<0.05, ***p<0.001, Kruskal-Wallis test with Dunn's post-test). **(B–E)** Western blot was also performed on total kidney cortex for phospho-β-catenin (Ser552), total-β-catenin, c-Myc, and GAPDH. Representative blots from three independent experiments are shown. Densitometry analysis was performed to quantify protein expression. (n=3, *p<0.05, **p<0.01, ***p<0.001, Kruskal-Wallis test with Dunn's post-test).

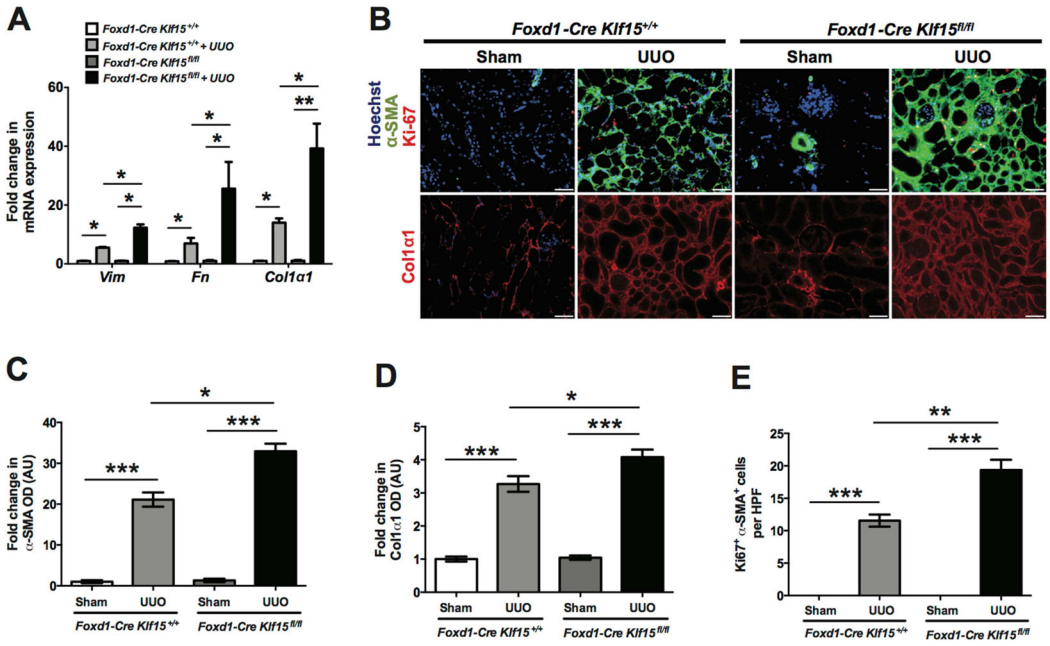

Figure 5. Loss of *Klf15* in Foxd1+ stromal cells increases the expression of fibrotic markers 7 days post UUO

Age-matched 12-week-old *Foxd1-Cre Klf15$^{fl/fl}$* and *Foxd1-Cre Klf15$^{+/+}$* mice were concurrently treated with UUO or sham for 7 days. **(A)** RNA was extracted from total kidney cortex and RT-PCR was performed for *Vimentin (Vim), Fibronectin (Fn),* and *Col1α1* expression. (n=6, *p<0.05, **p<0.01, Kruskal-Wallis test with Dunn's post-test). **(B)** Immunostaining for α-SMA and Ki67 (top panel) and Col1α1 (bottom panel) was performed in all groups of mice. Representative images from four mice in each group are shown (X 20). ImageJ was used to quantify the area stained per high power field (HPF) as a relative fold change to sham-treated mice for **(C)** α-SMA and **(D)** Col1α1. **(E)** Quantification of myofibroblast proliferation was determined by quantifying the number of Ki67+ and α-SMA+ cells per HPF. (n=6, *p<0.05, **p<0.01, ***p<0.001, Kruskal-Wallis test with Dunn's post-test).

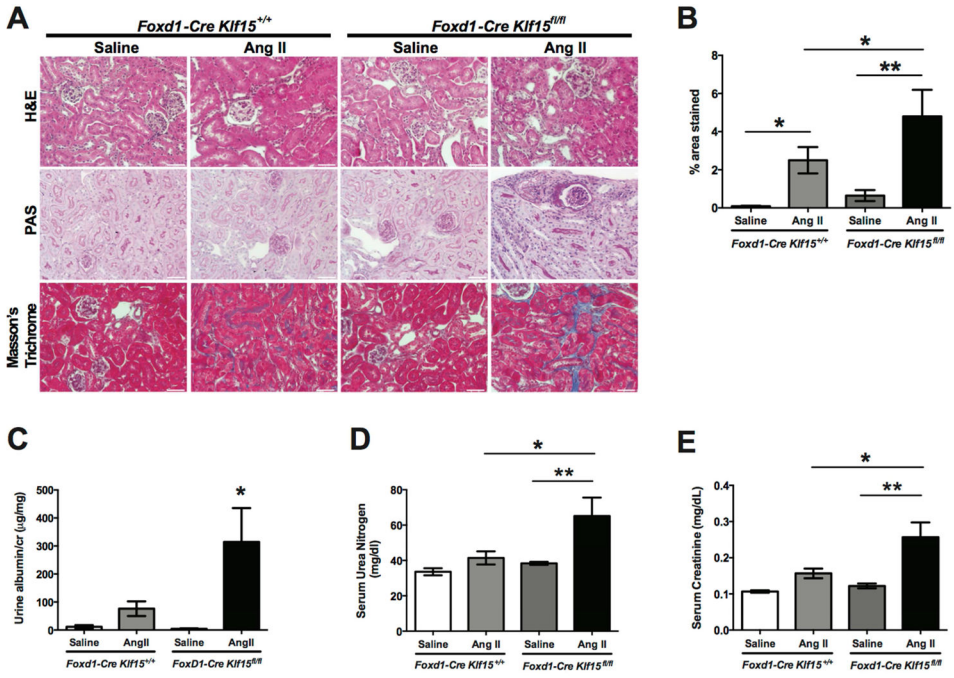

Figure 6. Loss of *Klf15* in Foxd1+ stromal cells exacerbates AngII-induced fibrosis

Age-matched 12-week-old *Foxd1-Cre Klf15$^{fl/fl}$* and *Foxd1-Cre Klf15$^{+/+}$* mice were concurrently treated with saline or AngII continuous infusion for 6 weeks. **(A)** All mice were sacrificed and renal cortex fixed for histology. Hematoxylin and Eosin (H&E), Periodic acid-Schiff (PAS), and Masson's Trichrome staining was performed to evaluate for tubulointerstitial changes. The representative images from 6 mice in each group are shown (X 20). **(B)** % area fibrosis from Masson's Trichrome stain is shown. **(C)** Urine albumin to creatinine (cr), **(D)** Serum urea nitrogen, and **(E)** Serum creatinine were measured in all 4 groups 6 weeks post treatment. (n=6, *p<0.05, **p<0.01, Kruskal-Wallis test with Dunn's post-test).

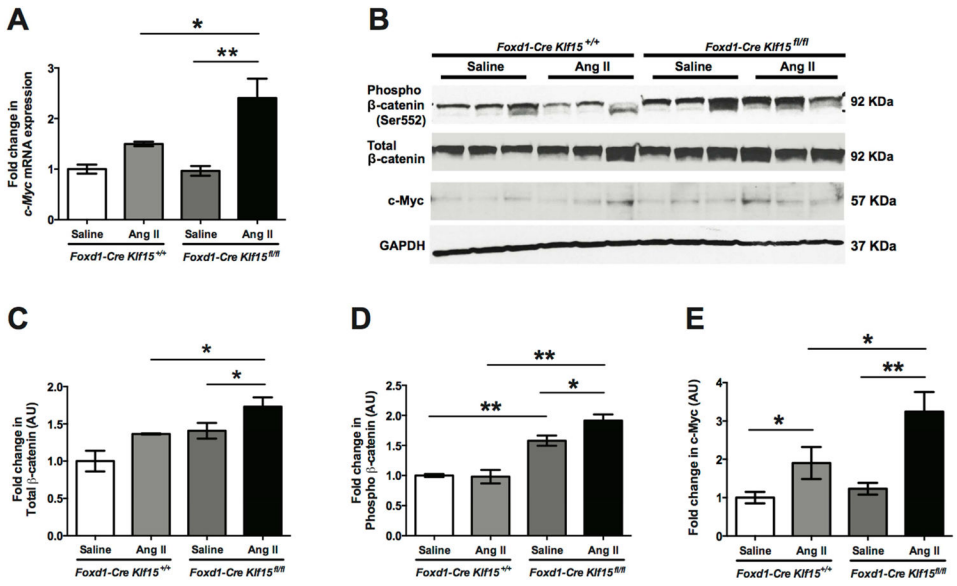

Figure 7. Activation of Wnt/β-catenin signaling in AngII-treated *Foxd1-Cre Klf15*$^{fl/fl}$ mice

(A) RNA was extracted from total kidney cortex and RT-PCR was performed for c-Myc expression from 12-week-old *Foxd1-Cre Klf15*$^{fl/fl}$ and *Foxd1-Cre Klf15*$^{+/+}$ mice treated with saline or AngII for 6 weeks. (n=6, *p<0.05, **p<0.01, Kruskal-Wallis test with Dunn's post-test). **(B–E)** Western blot was also performed on total kidney cortex for phospho-β-catenin (Ser552), total-β-catenin, c-Myc, and GAPDH. Representative blots from three independent experiments are shown. Densitometry analysis was performed to quantify protein expression. (n=3, *p<0.05, **p<0.01, Kruskal-Wallis test with Dunn's post-test).

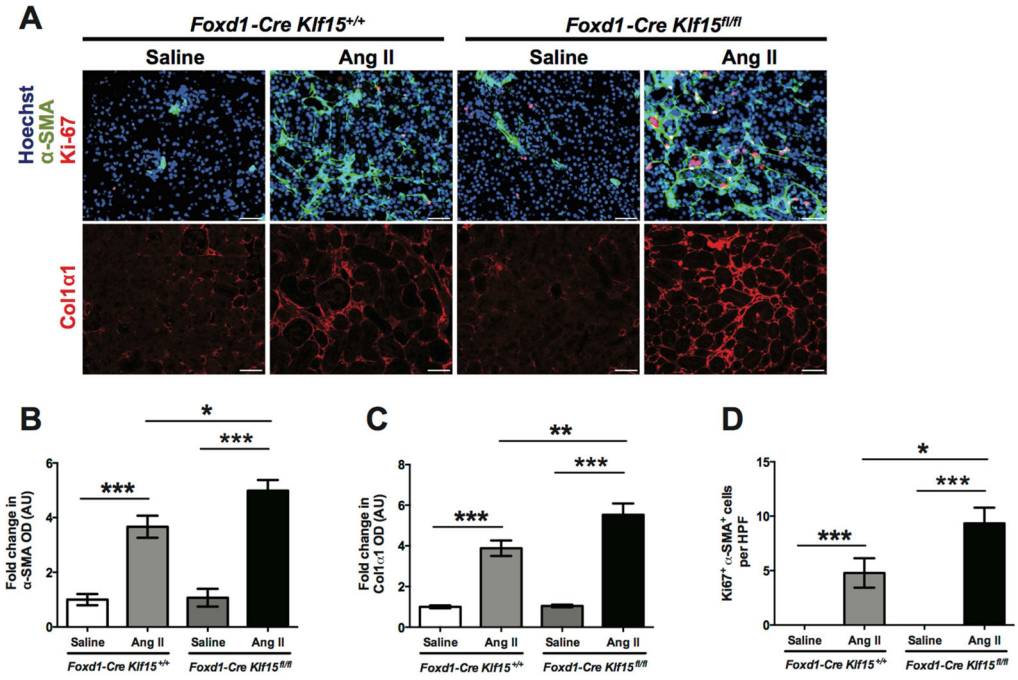

Figure 8. Loss of *Klf15* in Foxd1+ stromal cells increases the expression of fibrotic markers post AngII infusion

Age-matched 12-week-old *Foxd1-Cre Klf15$^{fl/fl}$* and *Foxd1-Cre Klf15$^{+/+}$* mice were concurrently treated with saline or AngII for 6 weeks. **(A)** Immunostaining for α-SMA and Ki67 (top panel) and Col1α1 (bottom panel) was performed in all groups of mice. Representative images from four mice in each group are shown (X 20). ImageJ was used to quantify the area stained per high power field (HPF) as a relative fold change to saline-treated *Foxd1-Cre Klf15$^{+/+}$* mice for **(B)** α-SMA and **(C)** Col1α1. **(D)** Quantification of myofibroblast proliferation was determined by quantifying the number of Ki67+ and α-SMA+ cells per HPF. (n=6, *p<0.05, **p<0.01, ***p<0.001, Kruskal-Wallis test with Dunn's post-test).

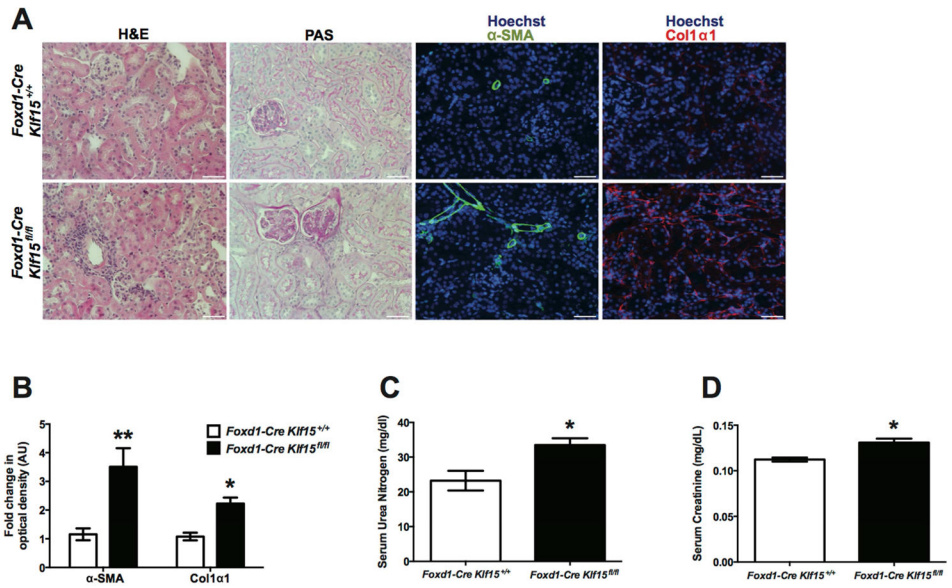

Figure 9. Older *Foxd1-Cre Klf15$^{fl/fl}$* mice exhibit an increase in fibrotic markers with renal dysfunction

Foxd1-Cre Klf15$^{fl/fl}$ and *Foxd1-Cre Klf15$^{+/+}$* littermates were aged for 52 weeks and were subsequently sacrificed to evaluate for tubulointerstitial changes. Renal cortex was fixed for histology and stained for Hematoxylin and Eosin (H&E) and Periodic acid-Schiff (PAS). The representative images from 4 mice in each group are shown (X 20). **(B)** Serum urea nitrogen and **(C)** Serum creatinine were measured in age-matched mice. (n=6, *p<0.05, **p<0.01, Mann-Whitney test).

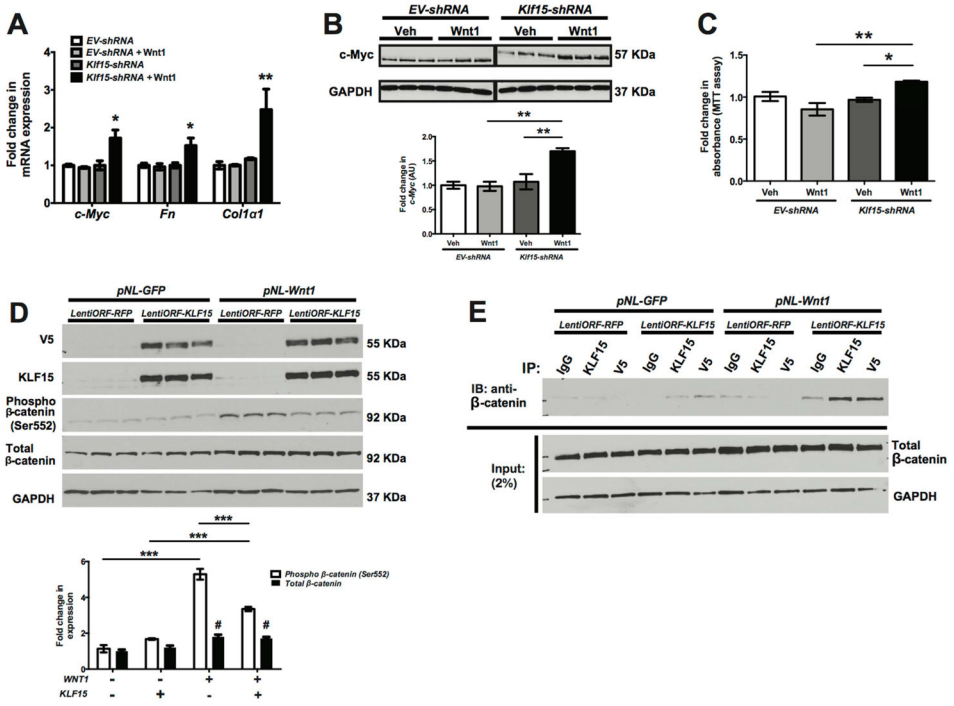

Figure 10. Modulating Klf15 expression in MEFs regulates Wnt/β-catenin signaling

Klf15 knockdown (*Klf15-shRNA*) in MEFs was performed using lentiviral shRNAmir system. *EV-shRNA* serves as the empty vector control. **(A)** *Klf15-shRNA* and *EV-shRNA* were treated with Wnt1 ligand (supernatant collected from pNL-CMVWnt1IRESEGFP-WPREΔU3 HEK293 cells) or vehicle (supernatant collected from pNL-CMVIRESEGFP-WPREΔU3 HEK293 cells) for 48 hours. RNA was extracted and RT-PCR was performed for *c-Myc*, *Fibronectin (Fn),* and *Col1α1*. **(B)** Western blot was also performed on protein lysates for c-Myc and GAPDH. Representative blots from three independent experiments are shown. Densitometry analysis was performed to quantify protein expression. **(C)** Cell proliferation was also measured using MTT assay in *Klf15-shRNA* and *EV-shRNA* cells treated with Wnt1 ligand or vehicle for 48 hours. Initially, stable Wnt1 expressing HEK293 cells (*pNL-Wnt1*) were generated. *pNL-GFP* serves as vector control for Wnt1 expressing cells. Subsequently, *KLF15* was transiently overexpressed in HEK293 cells using V5-tagged *lentiORF-KLF15* clone. *LentiORF-RFP* serves as vector control. **(D)** 48 hours after *KLF15* overexpression, western blot was performed for V5, KLF15, phospho-β-catenin (Ser552), total-β-catenin, and GAPDH. Representative blots from three independent experiments are shown with densitometry analysis to quantify protein expression in the bottom panel. (n=3, *p<0.05, **p<0.01, Kruskal-Wallis test with Dunn's post-test). **(E)** To demonstrate the interaction with KLF15 and β-catenin, co-immunoprecipitation (co-IP) was performed with initial immunoprecipitation of KLF15 with anti-V5 antibody and anti-KLF15 antibody and subsequently measuring β-catenin. IgG isotype serves as control for IP and GAPDH serves as loading control.

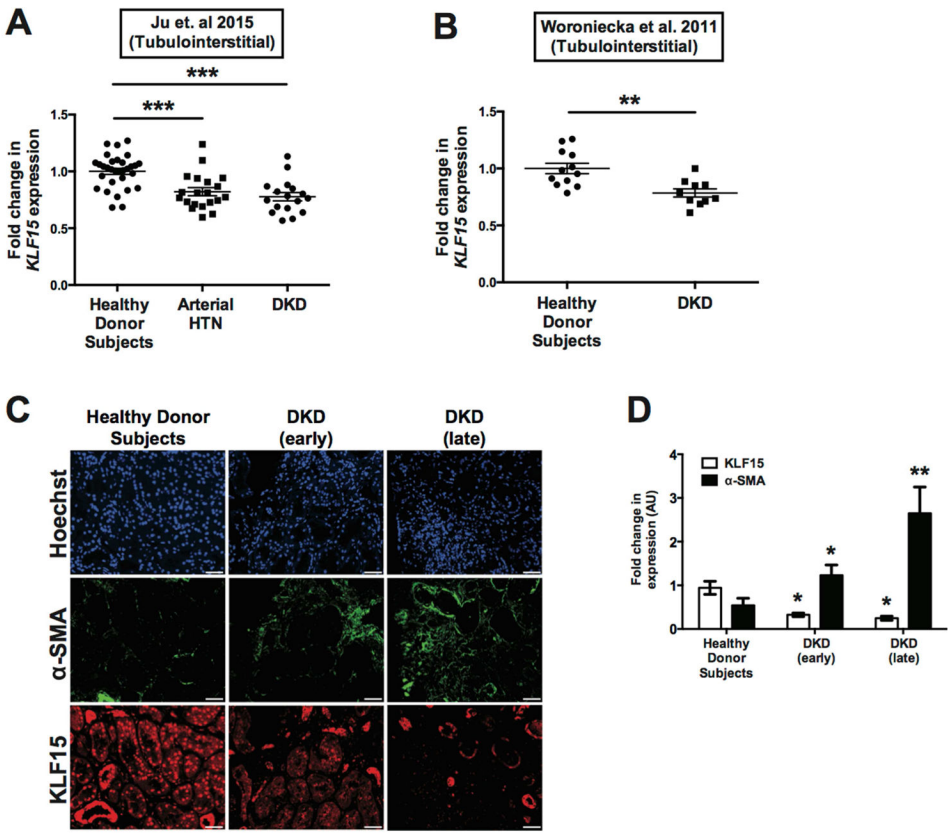

Figure 11. Reduced KLF15 expression in human kidney biopsies with fibrosis

(A) Previously reported gene expression arrays from Ju et al. [29] were utilized to examine *KLF15* expression in RNA from microdissected tubulointerstitial compartments of kidney biopsies with arterial hypertension (HTN), diabetic kidney disease (DKD) as compared to healthy donor subjects (***p<0.01, Kruskal-Wallis test with Dunn's post-test). **(B)** KLF15 expression was also examined in microdissected tubulointerstitial compartments of kidney biopsies with DKD as compared to healthy donor subjects from Woroniecka et al. [28] (**p<0.01, Mann-Whitney test). **(C)** Immunostaining for KLF15, α-SMA, and Hoechst were performed in kidney biopsies with early-stage DKD, late-stage DKD, and healthy donor nephrectomies. **(D)** ImageJ was used to quantify the intensity of expression in all three groups. (n=6, *p<0.05, **p<0.01, Kruskal-Wallis test with Dunn's post-test).